ELSEVIER

Applied Catalysis B: Environmental 4 (1994) 167–186

applied catalysis B

Reduction of sulfur dioxide by carbon monoxide to elemental sulfur over composite oxide catalysts

Wei Liu, Adel F. Sarofim, Maria Flytzani-Stephanopoulos[1,*]

Department of Chemical Engineering, Massachusetts Institute of Technology, Cambridge, MA 02139, USA

Received 29 December 1993; revised 25 March 1994; accepted 25 March 1994

Abstract

The catalyst activity of fluorite-type oxide, such as ceria and zirconia, for the reduction of sulfur dioxide by carbon monoxide to elemental sulfur can be significantly promoted by active transition metals, such as copper. More than 95% elemental sulfur yield, corresponding to almost complete sulfur dioxide conversion, was obtained over a Cu–Ce–O oxide catalyst with a feed gas of stoichiometric composition ($[CO]/[SO_2]=2$) at temperatures above 450°C. This type of mixed metal oxide catalyst has stable activity and is resistant to water and carbon dioxide poisoning. XPS analysis found copper in the Cu–Ce–O oxide in a reduced oxidation state (Cu^{1+}, Cu^0). The stable fluorite-type structure, regarded as the backbone structure of the catalyst, existed in both the fresh and the spent catalyst. The high activity resulted from the strong interaction of transition metal and fluorite oxide.

Keywords: Copper–cerium oxide; Elemental sulfur production; Fluorite oxide; Reduction; Sulfur dioxide

1. Introduction

Desulfurization of combustion exhaust gases is presently a costly process often involving complex flowsheets and "throw-away" sorbents. Directly reducing sulfur dioxide to elemental sulfur over a catalyst is attractive, because it produces a salable product without any solid waste to dispose of. Direct flue gas reduction processes involve non-selective catalysts, thus consuming large amounts of reductant (H_2 or CO) to react the excess oxygen in the exhaust gas. Additionally, these processes require an expensive Claus plant to complete the elemental sulfur recovery [1,2]. Other processes under development are two-stage, dry regenerative flue gas cleanup processes, whereby dilute SO_2 streams are scrubbed by reaction with

*Corresponding author.

[1]Present address: Department of Chemical Engineering, Tufts University, Medford, MA 02155

SSDI 0926-3373(94)00019-B

a metal oxide sorbent and the spent sorbent is regenerated for re-use with concomitant emission of a concentrated SO_2 stream suitable for sulfur recovery. The regenerator off-gas has only a fraction of the flue gas volume, and contains no oxygen. Recovery of sulfur from this type of gas in a single-stage catalytic converter, avoiding the multistage Claus plant, would decrease the cost and accelerate the commercialization of dry regenerative flue gas cleanup processes.

The direct reduction of SO_2 by CO to elemental sulfur has long been known, but, no substantial commercial experience exists. The overall reactions involved in this process are as follows:

$$SO_2 + 2CO \rightarrow 2CO_2 + 1/xS_x \quad (1)$$

$$CO + 1/xS_x \rightarrow COS \quad (2)$$

$$2COS + SO_2 \rightarrow 2CO_2 + 3/xS_x \quad (3)$$

where $x = 2$–8 or higher. At high temperatures, predominantly gaseous elemental sulfur, S_2, produced through Eq. (1) can react with carbon monoxide to form carbonyl sulfide, COS, which may again reduce SO_2 to elemental sulfur through reaction (3). However, COS is a more toxic compound than SO_2 and its production should be minimized in a sulfur recovery process. In addition to the formation of undesirable COS, the presence of water vapor impurity in the feed gas may have a major effect on both the catalyst activity and product selectivity by poisoning the catalyst and/or promoting the following reactions:

$$CO + H_2O \rightarrow H_2 + CO_2 \quad (4)$$

$$COS + H_2O \rightarrow H_2S + CO_2 \quad (5)$$

$$H_2 + [S] \rightarrow H_2S \quad (6)$$

$$3/xS_x + 2H_2O \rightarrow 2H_2S + SO_2 \quad (7)$$

Reactions (1)–(7) have favorable thermodynamics at the conditions of interest to this work (atmospheric pressure, 300 to 700°C). The challenge to realize the one-stage elemental sulfur recovery scheme is to develop a catalyst which is not poisoned by water or other gas impurities and to maximize the yield of elemental sulfur.

Alumina-supported transition metals, such as Cu, Fe, Ni, Pd, etc., have been extensively studied for the reduction of sulfur dioxide by carbon monoxide [3–9]. The production of COS usually proceeds to a substantial extent on these catalysts and water partially poisons the catalyst activity. Lower COS formation was realized on mixed oxides of elements from the lanthanide group and the groups of IVA and VA [10–12], such as La–Ti–O. But, this type of catalyst typically needs to be activated by reducing gases at high temperature. Perovskite-type mixed oxides [13–16], ABO_3, containing transition metals in position B and rare earth and/or alkaline earth elements in position A, were found as active catalysts with high selectivity to elemental sulfur over COS. However, this type of catalyst, for exam-

ple, $La_{1-x}Sr_xCoO_3$ [15], essentially lost its perovskite structure after a short induction period under reaction conditions and became a mixture of metal sulfides and oxysulfides which contributed to the catalyst activity as suggested by Baglio [17]. In addition, the water vapor effects on these catalysts have not been reported.

A redox reaction mechanism involving the participation of surface oxygen/oxygen vacancy has been proposed for the SO_2 reduction by CO [12,15]. We recently reported that cerium oxide, a fluorite oxide well known for its high oxygen vacancy concentration and mobility, is an active catalyst and its activity can be further enhanced by doping it with lanthanum oxide [18]. However, alkaline and rare earth oxide dopants did not improve the resistance of ceria towards water poisoning. In the present study, we have modified the ceria with transition metals, examined other oxygen-ion conducting materials as potential catalysts, and evaluated the catalyst activity and selectivity as a function of catalyst type and operating conditions, including the effect of water vapor.

2. Experimental

2.1. Apparatus and procedure

All catalysts were tested in a laboratory-scale, packed bed flow reactor, consisting of a 0.6 cm I.D. × 50 cm long quartz tube with a porous quartz frit placed at the middle for supporting the catalyst. The reactor tube was heated by a Lindberg furnace. The reaction temperature was monitored by a quartz tube-sheathed K-type thermocouple placed at the top of the packed bed and controlled by a Wizard temperature controller. The reacting gases, all certified calibration gas mixtures with helium (Matheson), were measured with rotameters and mixed prior to the reactor inlet. The resulting gas mixture flowed downward through the packed bed. Water vapor was introduced with helium bubbling through a heated water bath. The pressure drop of gas flowing through the assembly was small. Thus, experiments were carried out at nearly atmospheric pressure. A cold trap installed at the outlet of the reactor was used to condense out the elemental sulfur from the product gas stream. The product gas, free of sulfur and particulates, was analyzed by a HP5880A gas chromatograph (GC) with a thermal conductivity detector (TCD). Helium was used as the GC carrier and reference gas, each at 30 cm^3/min. The detector and oven temperatures were set at 200°C and 60°C, respectively. A 1/4 in. O.D. × 6 ft. long packed column of Chromosil 310 (from SUPELCO) provided good separation of CO, CO_2, COS, H_2S, CS_2, and SO_2 under these conditions. The TCD showed linear response to all the compounds mentioned above and a detection limit of less than 100 ppm by volume.

A fresh catalyst was evaluated by a two-step test procedure. In the first step, the reactant gas mixture was introduced into the reactor at about 500°C and the reaction temperature was raised by about 50°C increments after a steady-state reaction was

reached at each temperature. The reaction light-off temperature was thus identified, at which the reaction occurred with SO_2 conversion exceeding 90%. In the second step, the reaction temperature was lowered in steps of about 50°C from a high temperature until conversion was significantly decreased. Hysteresis effects between the light-off and fall-off branches were followed in this sequence of steps.

The effect of water on the catalyst activity and selectivity was examined by adding about 2% by volume of water vapor into the reactant gas mixture. Unless specifically noted, catalyst tests were typically performed with 150 mg catalyst loaded in the reactor, gas flow-rate set at 100 sccm and comprising 1% SO_2, 2% CO by volume, and balance helium. The contact time was 0.09 $g \times s/cm^3$ (STP). Each catalyst had a different packing density so that the space velocity varied with the individual catalyst tested. Sulfur dioxide conversion, X-SO_2, and elemental sulfur yield, Y-sulfur, are defined by following equations:

$$X\text{-}SO_2 = \{[SO_2]_o - [SO_2]\}/[SO_2]_o$$

$$Y\text{-sulfur} = [S]/[SO_2]_o$$

where $[SO_2]_o$ and $[SO_2]$ are the inlet and outlet sulfur dioxide concentrations, respectively, while [S] is the outlet elemental sulfur concentration calculated from the material balance of carbon and sulfur, and occasionally checked by titration of the sulfur collected in the cold trap.

2.2. *Catalyst preparation*

Both bulk composite and impregnated oxide catalysts were prepared in this study. The composite catalysts were prepared by coprecipitating aqueous salt solutions of the metals with ammonium carbonate. The precipitates were washed twice with hot deionized water and then dried for about 12 hours at 110°C. The dried samples were further heated for a few hours in stagnant air at 650°C. The particle sizes used for tests were -35 + 100 mesh (420–149 mm) except for tests with zirconia catalysts where -250 mesh (<63 mm) particles were used. The supported catalysts were prepared by conventional wet impregnation of the support with aqueous salt solutions of the metals. The slurry of the support and solution was degassed in vacuum so that the salt solution fully filled the pores of the support during impregnation. Then, the excess solution was filtered. The wetted samples were dried for two days at room temperature and then heated for four hours at 650–700°C in a muffle furnace. The metal content in the impregnated catalysts was determined with inductively coupled plasma (ICP) atomic emission spectrometry (Perkin-Elmer Plasma 40). The $Cu/\gamma\text{-}Al_2O_3$ catalyst was prepared by reduction of $CuO/\gamma\text{-}Al_2O_3$ with 10% CO/He at 300°C. The materials used in catalyst preparation are listed in Table 1.

Catalyst characterization was performed by X-ray powder diffraction on a Rigaku 300 X-ray diffractometer for crystalline phase identification, by N_2 desorption on a Micromeritics FlowSorb II 2300 apparatus for BET surface area measurement,

Table 1
Materials inventory used for catalyst preparation

Materials	Source
Chemicals	
Cerium nitrate hexahydrate, containing 1.38 wt.-% lanthanum	Aldrich
Cerium acetate hydrate, 99.9%	Aldrich
Cobalt^{II} nitrate hydrate, 99.99%	Aldrich
Terbium^{III} nitrate pentahydrate, 99.9%	Aldrich
Yttrium nitrate pentahydrate, 99.9%	Aldrich
Hydrogen hexachloroplatinate^{IV} hydrate, A.C.S. grade	Aldrich
Chromium^{III} nitrate, 98.5%	Johnson Matthey
Copper^{II} nitrate, A.C.S. grade	Johnson Matthey
Gadolinium nitrate, 99.9%	Johnson Matthey
Zirconium dichloride oxide, 99.9%	Johnson Matthey
Ammonium carbonate, A.C.S. grade	Fisher Scientific
Nickel nitrate, A.C.S. grade	Fisher Scientific
Manganese^{II} nitrate tetrahydrate, 98%	Fluka
Support	
CeO_2	Thermal decomposition of cerium acetate at 750°C
CeO_2 particle sizes: 500 to 150 μm	
CeO_2 surface area: 24 m^2/g	
CeO_2 void fraction: ca. 0.12 cm^3/g	
CeO_2 packed density: 0.95 g/cm^3	
γ-Al_2O_3	LaRoche
γ-Al_2O_3 particle size: 72 μm average	
γ-Al_2O_3 surface area: 300 m^2/g	
γ-Al_2O_3 void fraction: ca. 1.0 cm^3/g	
γ-Al_2O_3 packed density: 0.6 g/cm^3	

and by scanning electron microscopy (SEM) on a Cambridge Stereoscan 240 MK.3 for catalyst morphology observation. Elemental distribution was examined by scanning transmission electron microscopy (STEM) using a Vacuum Generators HB603 instrument, while X-ray photoelectron spectroscopy (XPS) of the catalyst surface was performed with a Perkin-Elmer 5100 instrument. For STEM analysis, the fine catalyst powder was embedded in a resin matrix, the resin was ultramicrotomed to slices of 80 to 120 nm, and the slices were supported on a nickel grid and coated with carbon.

3. Results

3.1. Transition metal-impregnated ceria catalysts

Fig. 1 shows the light-off curves of sulfur dioxide reaction with carbon monoxide over the transition metal-impregnated ceria catalysts. The light-off temperatures are 500°C on the Cu/CeO_2 and Ni/CeO_2 catalysts, 550°C on the Pt/CeO_2, and

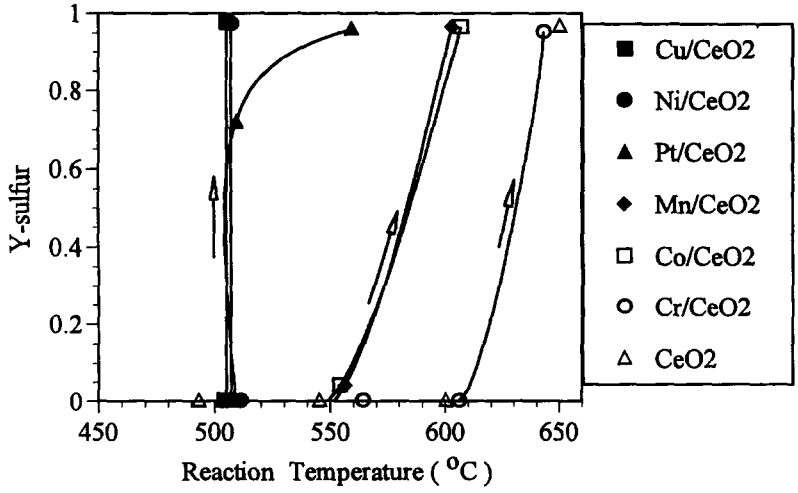

Fig. 1. Light-off behavior on the transition metal-impregnated ceria catalysts (1% SO_2, 2% CO, 97% He).

600°C on the Co/CeO_2 and Mn/CeO_2. A light-off temperature higher than 600°C was found for unmodified ceria and for Cr/CeO_2 catalysts. Thus, addition of transition metals significantly lowered the light-off temperature of ceria. The fall-off behavior on these catalysts as well as water vapor effects are plotted in Fig. 2. In these tests, ceria and Cr/CeO_2 were activated by reduction with 10% CO/He at 600°C. The reaction starts to fall off around 550°C on ceria and below 500°C on the other catalysts. The Cr/CeO_2 shows a low fall-off temperature, although it was difficult to activate it in the reaction mixture (Fig. 1). However, this catalyst completely deactivated upon addition of water at 550°C as did ceria. The other catalysts were still active in the presence of water. The sulfur yield at 510°C was higher on the Cu-, Co- and Ni-impregnated ceria catalysts (ca. 0.7) than on the

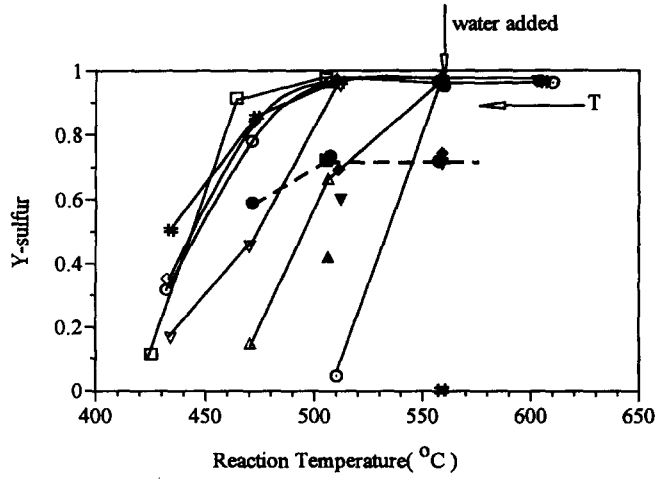

Fig. 2. Fall-off behavior and water vapor effect on the transition metal-impregnated ceria catalysts. (□) Cu/CeO_2, (◇) Ni/CeO_2, (△) Pt/CeO_2, (▽) Mn/CeO_2, (○) Co/CeO_2, (#) Cr/CeO_2, (⊙) CeO_2. Open symbols for dry gas (1% SO_2, 2% CO, 97% He), filled symbols for wet gas (1% SO_2, 2% CO, 2% H_2O, 95% He).

Table 2
Transition metal-impregnated ceria catalysts

Catalyst		Light-off	Y-sulfur/X-SO_2[f]	
Composition	Surface area (m^2/g)	$T_{90\%}$[c] (°C)	Dry gas[d] (510°C)	Wet gas[e] (510°C)
CeO_2	24	>600	0.04/0.12	0.0/0.0
Cu/CeO_2[a]	21.4	500	0.97/0.99	0.73/0.91
Ni/CeO_2[a]	22.7	500	0.97/0.98	0.69/0.78
Pt/CeO_2[b]	22.9	550	0.66/0.68	0.42/0.44
Mn/CeO_2[a]	20.8	600	0.95/0.97	0.60/0.66
Co/CeO_2[a]	22.5	600	0.96/0.98	0.73/0.88
Cr/CeO_2[a]	16.3	>600	0.96/0.97	0.0/0.0

[a]CeO_2 was impregnated with 0.5 *M* metal nitrate solution. The atomic transition metal content in the resulting catalyst (nM/(nM+nCe)×100%) is about 13%.
[b]CeO_2 was impregnated with 10 mg Pt/cm^3 hydrogen hexachloroplatinate^{IV} hydrate solution.
[c]Reaction temperature at which 90% conversion occurred during temperature-rise test.
[d]Reacting gas mixture consisted of 1% SO_2, 2% CO, balance helium.
[e]2% H_2O was added into reacting gas mixture.
[f]Sulfur yield/SO_2 conversion; see text.

Mn- and Pt-impregnated ceria (0.4–0.6). Table 2 lists the numerical values of sulfur yield and SO_2 conversion in tests with the dry and wet reactant gas mixtures shown in Figs. 1 and 2. It is seen that in the dry gas almost all the sulfur dioxide was converted to elemental sulfur. However, the elemental sulfur yield decreased from a typical 0.96 (dry gas) to 0.4–0.7 (wet gas) due to the formation of hydrogen sulfide.

Fig. 3 shows the variation of gaseous product distribution with time-on-stream on the Cu/CeO_2 catalyst at 510°C in the presence of water. Formation of H_2S

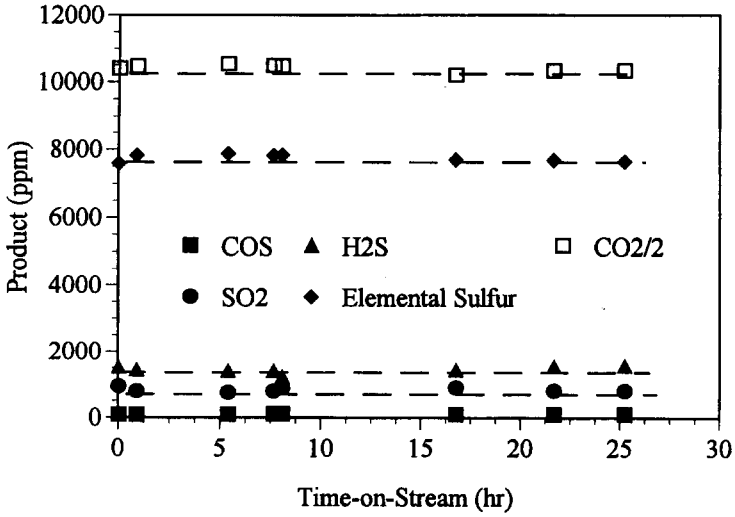

Fig. 3. Long-term test of Cu/CeO_2 catalyst in wet gas (1% SO_2, 2% CO, 2% H_2O, 95% He), 100 sccm, 505°C, 307 mg catalyst loading.

according to reactions (4) and (6) consumed some reductant CO, resulting in a sub-stoichiometric amount for the reduction of SO_2. The ratio of H_2S to SO_2 concentration in the product gas was around stoichiometric, which means that nearly complete conversion of the inlet CO took place. Fig. 3 also indicates that the Cu/CeO_2 catalyst is stable under the reacting conditions, since no apparent deactivation was observed during a 25-hour run. This promising catalyst system was used for detailed studies of the SO_2 reaction with CO.

3.2. *Effect of copper content on the catalyst activity and selectivity of the Cu–Ce–O system*

Two series of Cu–Ce–O catalysts, listed in Table 3, were prepared by coprecipitation and impregnation methods, respectively, to evaluate the effect of copper content on the catalyst activity and selectivity. The La-doped ceria and alumina-supported copper catalysts are also included in Table 3 for comparison. The bulk Cu–Ce–O composite catalyst typically has a surface area around 30 m^2/g, while the impregnated ceria catalyst has a surface area slightly lower than the CeO_2 support (24 m^2/g). The Cu/Al_2O_3 catalysts have much higher surface area (ca.

Table 3
Variation of catalyst activity and selectivity with catalyst composition in the Cu–Ce–O system

Catalyst		Y-sulfur/X-SO_2[f]			
Composition	Surface area(m^2/g)	Dry gas[d]		Wet gas[e]	
		465°C	510°C	470°C	510°C
Composite catalyst[a]					
$La_{0.1}Ce_{0.9}O_x$	28.5	0.06/0.20	0.97/1.00	–	0.0/0.0
$Cu_{0.01}Ce_{0.99}(La)O_x$	57.0	0.97/1.00	0.97/1.00	0.65/0.81	0.66/0.90
$Cu_{0.05}Ce_{0.95}(La)O_x$	57.0	0.83/0.92	0.95/0.98	0.53/0.71	0.61/0.87
$Cu_{0.15}Ce_{0.85}(La)O_x$	30.7	0.97/0.99	0.97/1.00	0.69/0.90	–
$Cu_{0.2}Ce_{0.8}(La)O_x$	37.1	0.86/0.89	0.93/0.96	0.72/0.89	0.73/0.91
$Cu_{0.25}Ce_{0.75}(La)O_x$	30.2	0.93/0.97	0.94/1.00	0.64/0.84	0.69/0.92
$Cu_{0.35}Ce_{0.65}(La)O_x$	33.8	0.93/0.98	0.94/1.00	0.67/0.88	–
Impregnated catalyst[b]					
CeO_2 support	24.0	0/0.0	0.04/0.12	–	0.0/0.0
3.5 wt.-% CuO_x/CeO_2	22.0	0.93/0.97	0.94/1.00	0.60/0.77	0.73/0.93
7.8 wt.-% CuO_x/CeO_2	21.0	0.84/0.92	0.95/0.99	0.56/0.73	0.68/0.91
21 wt.-% CuO/γ-Al_2O_3	137	0.38/0.42	0.56/0.57	–	–
Cu/γ-Al_2O_3[c]	137	–	0.77/0.81	–	0.38/0.61

[a]Catalysts were prepared by coprecipitation. (La) denotes that the cerium nitrate precursor used contained about 1.38 wt.-% lanthanum.
[b]Catalysts were prepared by impregnation (wt.-% denotes the weight percent of copper).
[c]Prepared by reducing the 21 wt.-% CuO/γ-Al_2O_3 material with 10% CO/He at 300°C.
[d]Reacting gas mixture consisted of 1% SO_2, 2% CO, balance helium.
[e]2% H_2O was added into reacting gas mixture.
[f]Sulfur yield/SO_2 conversion; see text.

130 m^2/g) due to the γ-alumina support. Since the SO_2 conversion increases very fast with the reaction temperature, only experimental results at relatively low temperatures are included in Table 3 to compare the activity and selectivity. The light-off temperature on all the Cu–Ce–O catalysts was approximately 500°C, while the light-off temperatures on the Cu/Al_2O_3 catalysts and La-doped ceria were 560°C and 610°C, respectively.

The impregnated and bulk Cu–Ce–O catalysts show similar overall behavior and the catalyst activity is not sensitive to the copper content in the catalyst. However, there is a trend for the selectivity toward elemental sulfur to decrease as the copper content increases. In the presence of 2% water, hydrogen sulfide instead of carbonyl sulfide becomes a major byproduct over the Cu–Ce–O catalyst. The elemental sulfur yield drops from a typical 95% in the dry gas to about 70% in the wet gas. The Cu/γ-Al_2O_3 catalyst has a little higher activity than the CuO/γ-Al_2O_3, but, both catalysts are much less active than the Cu–Ce–O catalysts. Also, in contrast to the Cu–Ce–O, the copper/alumina catalyst favors the formation of COS in the presence of water as has been reported in the literature [8] and verified in this work.

3.3. Zirconate and zirconia catalysts

Zirconium oxide has the fluorite-type structure of ceria and is similar to ceria in many physical properties, such as high oxygen mobility and oxygen ion vacancy concentration, but, zirconia is much more difficult to reduce than ceria. Yttrium-stabilized zirconia is a well known oxygen ion conductor [19]. Mixed oxides of lanthanide elements and zirconium were reported by Bajars [10] as catalysts for sulfur dioxide reduction by CO. In addition, $Zr_2Ln_2O_7$-type zirconates (Ln = lanthanide element from La to Tb) of pyrochlore structure, notably, $Gd_2Zr_2O_7$, are known as another class of oxygen ion conductors [20].

Several zirconates (Ce, Tb, Gd) and zirconia-based oxides were prepared and tested in this work under similar conditions as the ceria-based catalysts. The results are summarized in Table 4. The zirconates have surface areas from about 30 to 50 m^2/g. Y-doped zirconia has much higher surface area than the Cu-doped zirconia, which may reflect the known stabilization effect yttrium imparts to the zirconia crystal structure. The zirconia-based catalysts consist largely of mesopores (tens of Å in diameter). Therefore, small particles, less than 63 μm, were used in the tests of the ZrO_2-based catalysts to overcome pore diffusion resistance. The light-off temperature over the Ce, Tb and Gd-zirconates was around 700°C, much higher than that for ceria. After the reaction was initiated at high temperature, however, the zirconate catalyst could maintain its high activity as the reaction temperature was lowered to 470°C. The performance of the $Gd_2Zr_2O_7$ catalyst system is shown in Fig. 4. More than 95% elemental sulfur yield was obtained over the temperature range 470 to 700°C in the dry gas. After the addition of 2 vol.-% water into the reactant gas at 560°C, the $Ce_2Zr_2O_7$ and $Tb_2Zr_2O_7$ catalysts were quickly deacti-

Table 4
Reduction of sulfur dioxide by carbon monoxide over zirconate and zirconia catalysts

Catalyst		Light-off	Y-sulfur/X-SO_2[d]	
Composition[a]	Surface area (m^2/g)	$T_{90\%}$ (°C)	Dry gas[b] (510°C)	Wet gas[c] (510°C)
$Gd_2Zr_2O_7$	37.8	700	0.95/0.99	0.0/0.0
$Tb_2Zr_2O_7$	50.8	700	0.97/0.99	–
$Ce_2Zr_2O_7$	37.0	700	0.96/1.00	–
$(Gd_2Zr_2)_{0.85}Cu_{0.15}O_x$	28.2	510	0.97/0.99	0.59/0.81
$Zr_{0.9}Y_{0.1}O_x$	41.7	610	0.54/0.58	–
$[Zr_{0.9}Y_{0.1}]_{0.85}Cu_{0.15}O_x$	65.0	510	0.87/0.90	–
$Zr_{0.8}Cu_{0.2}O_x$	17.8	510	0.92/0.96	0.70/0.87

[a]Catalysts were prepared by coprecipitation.
[b]Reacting gas mixture consisted of 1% SO_2, 2% CO, balance helium.
[c]2% H_2O was added into reacting gas mixture.
[d]Sulfur yield/SO2 conversion; see text.

vated; only the $Gd_2Zr_2O_7$ catalyst remained active. As the temperature was decreased to 510°C, this catalyst was also deactivated in the presence of water (Fig. 4). Therefore, $Gd_2Zr_2O_7$ is the most active among the three zirconate catalysts tested. The activity of this catalyst can be promoted by copper as indicated by the data of Table 4.

The yttria-doped zirconia catalyst, $Zr_{0.9}Y_{0.1}O_x$, has a 610°C light-off temperature, same as the La-doped ceria. The light-off temperature was lowered to 510°C by the addition of copper. The slightly lower SO_2 conversion observed on the Cu–Zr(Y)–O catalyst (Table 4) compared to Cu–Ce(La)–O at the same reaction temperature (Table 3) may be due to a pore diffusion limitation in the former catalyst system. Overall, zirconia is similar to ceria in its catalytic properties for the reduction of sulfur dioxide by carbon monoxide.

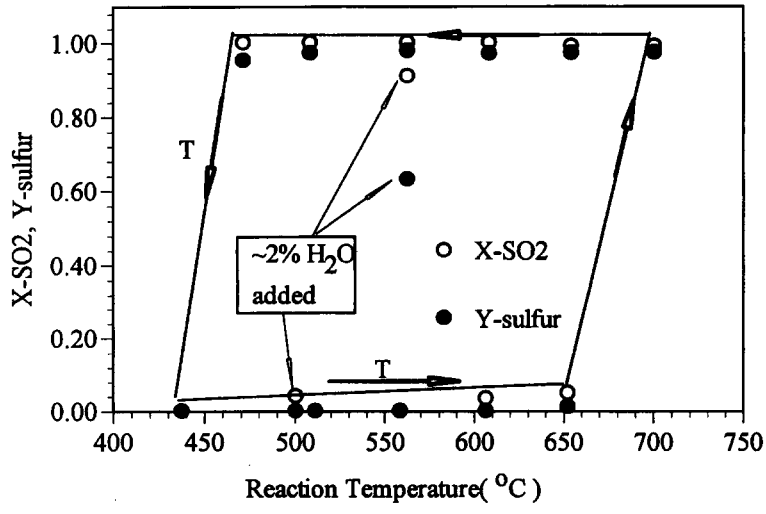

Fig. 4. SO_2 Reduction by CO over the $Gd_2Zr_2O_7$ catalyst (1% SO_2, 2% CO, 97% He).

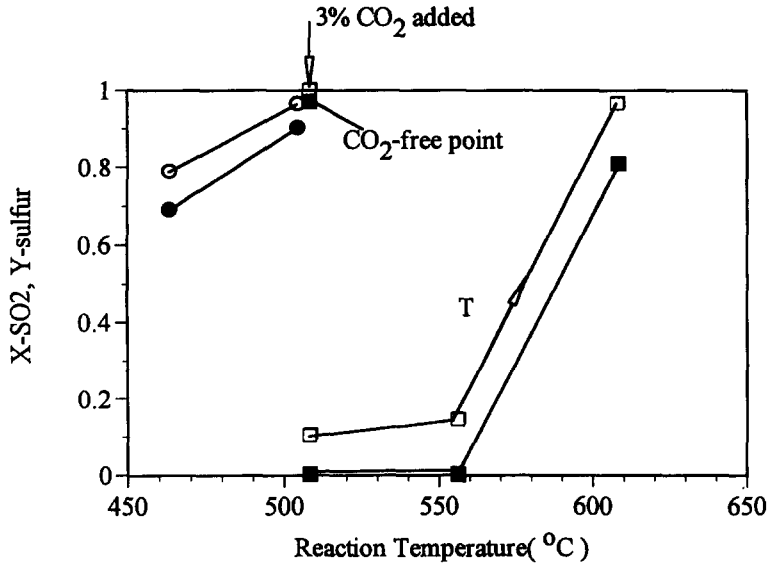

Fig. 5. Effect of CO_2 on catalyst activity and selectivity (1% SO_2, 2% CO, 3% CO_2, 94% He). X-SO_2: (□) $La_{0.1}Ce_{0.9}O_{1.95}$, (○) CU/CeO_2 Y-sulfur: closed symbols (■, ●).

3.4. *Effect of carbon dioxide on the catalytic activity and selectivity*

Carbon dioxide is produced by the present reaction and may also be present in the feed gas stream. Thus, its effect on catalyst activity and selectivity was briefly checked in this work. As shown in Fig. 5, addition of about 3% carbon dioxide into the reactant gas mixture at 510°C almost completely suppressed the reaction on the $Ce_{0.9}La_{0.1}O_x$ catalyst. The SO_2 conversion dropped from about 1.0 to 0.1, while the sulfur yield decreased from 0.96 to trace amounts. The catalyst activity was restored in the presence of carbon dioxide only when the temperature was raised to 600°C. However, the elemental sulfur yield was decreased to 0.81 because CO_2 lowered the SO_2 conversion and promoted the production of carbonyl sulfide (Fig. 5). In contrast, addition of CO_2 at 510°C did not suppress the reaction on the 7.8 wt.-% Cu/CeO_2 catalyst. This catalyst can maintain its activity even at the lower temperature of 465°C. Sulfur yield was decreased by a few percent as a result of promoted COS production and lower SO_2conversion. These results show that copper can enhance the resistance of the ceria catalyst to carbon dioxide poisoning.

Table 5
Variation of the $Cu_{0.15}Ce_{0.85}(La)O_x$ surface area with thermal treatment

	Fresh catalyst	Tested 12 h in dry gas[a] at ca. 500°C	Tested 37 h in wet gas[b] at ca. 500°C	Tested 18 h in dry gas[a] at ca. 750°C	Calcined 17 h in air at ca. 750°C
S_g (m^2/g)	30.7	26.4	26.8	22.8	22.6

[a]Dry reactant gas mixture consisted of 1% SO_2, 2% CO, balance helium.
[b]2% H_2O was added into the dry reactant gas mixture.

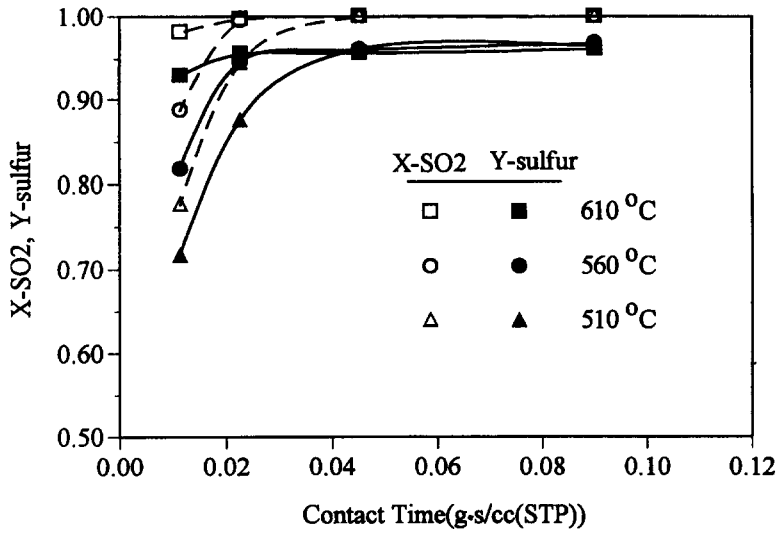

Fig. 6. Effect of contact time on SO_2 conversion at various temperatures: 1% SO_2, 2% CO, 97% He; $Cu_{0.15}Ce_{0.85}(La)O_x$ catalyst.

3.5. Bulk $Cu_{0.15}Ce_{0.85}(La)O_x$ catalyst

The $Cu_{0.15}Ce_{0.85}(La)O_x$ catalyst was chosen for further studies. This catalyst showed no apparent deactivation during a 35-hour run in the presence of 2% water at 470°C. The variation of surface area with temperature is shown in Table 5. Variation of conversion with contact time at different temperatures is plotted in Fig. 6. The conversion starts to decline from 0.99 at contact times shorter than

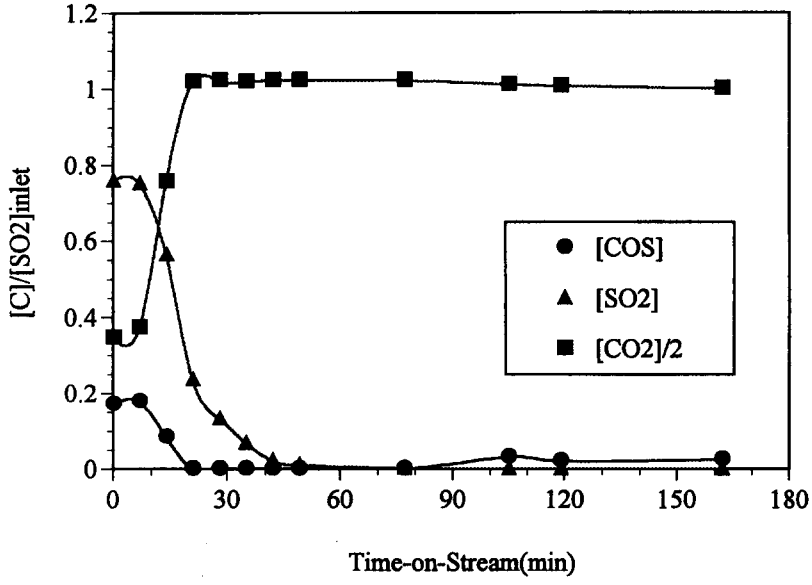

Fig. 7. Activation profile of $Cu_{0.15}Ce_{0.85}(La)O_x$ catalyst at 510°C (1% SO_2, 2.06% CO, balance helium).

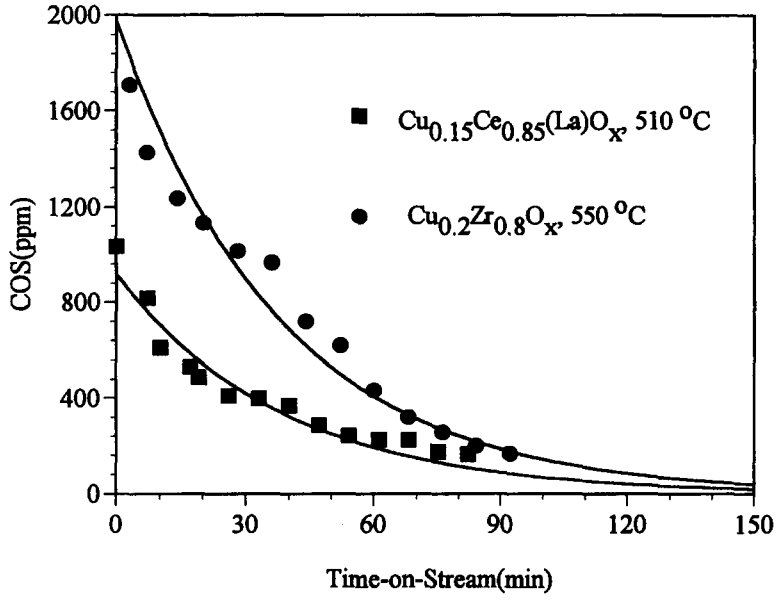

Fig. 8. COS Evolution profile during 2% CO/He scavenging of spent catalysts.

about 0.045 g×s/cm^3 (STP) at 510°C. No effect of contact time on selectivity was observed.

A fresh catalyst can be activated either by pre-reduction or starting the reaction at high temperature. Fig. 7 shows the activation profile of the $Cu_{0.15}Ce_{0.85}(La)O_x$ catalyst at 510°C in the reacting gas atmosphere. The consumption of CO in the

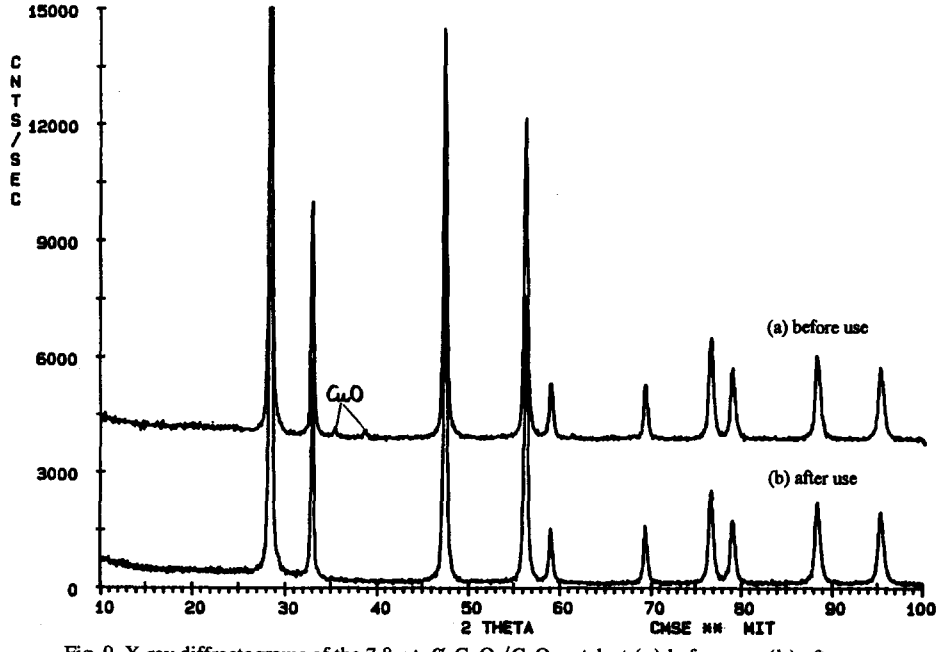

Fig. 9. X-ray diffractograms of the 7.8 wt.-% CuO_x/CeO_2 catalyst (a) before use; (b) after use.

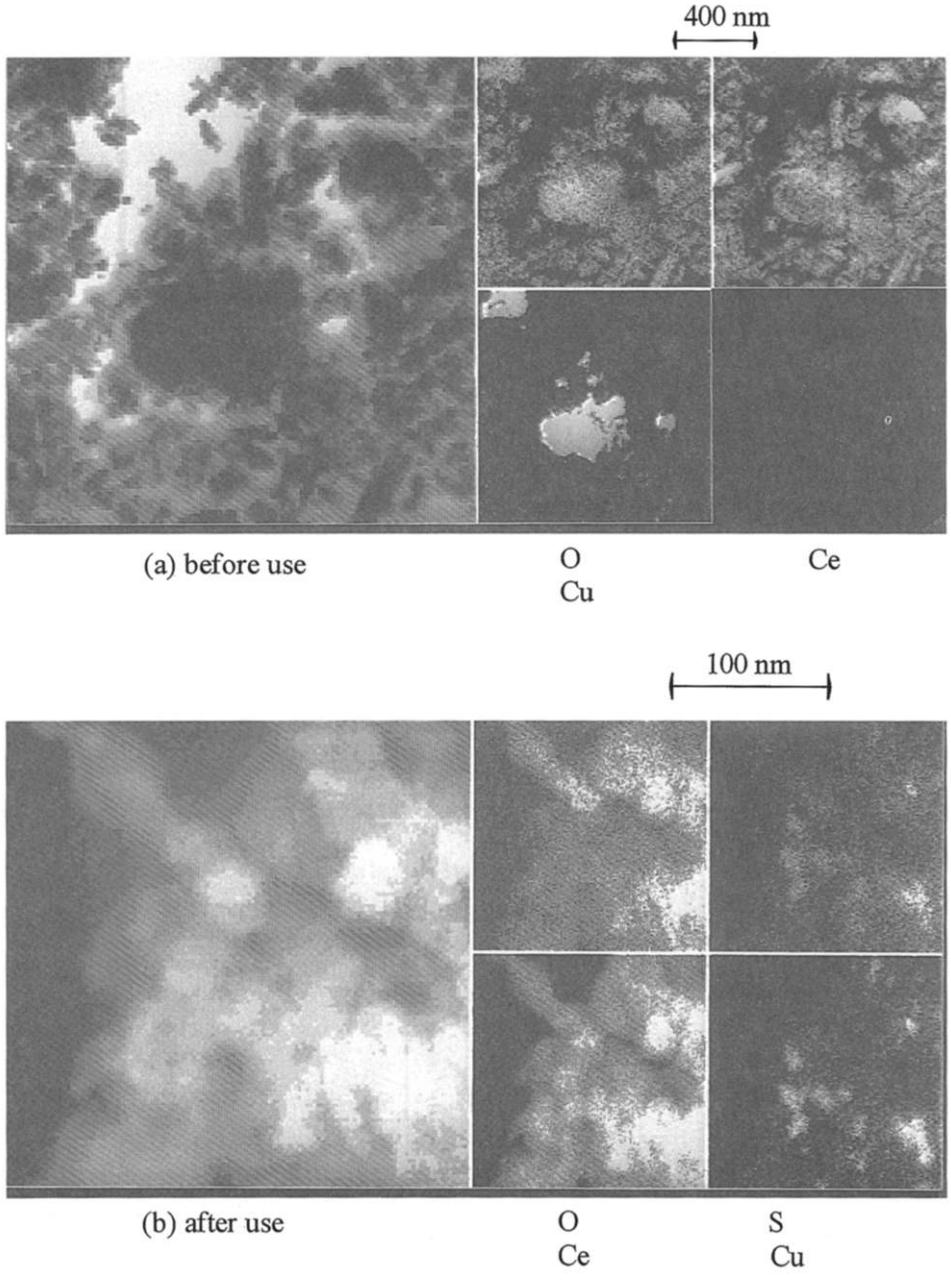

Fig. 10. STEM elemental mapping of the 7.8 wt.-% CuO_x/CeO_2 catalyst (a) before use; (b) after use.

transition region is more than what is required to reduce SO_2, which means that additional CO was consumed to reduce the catalyst and/or adsorbed oxidants on the catalyst surface. During activation, a significant amount of COS was observed. As the activation proceeded, COS decreased to zero and about 50 min later COS increased to a steady-state level of 300 ppm. Fig. 8 shows the COS evolution profile

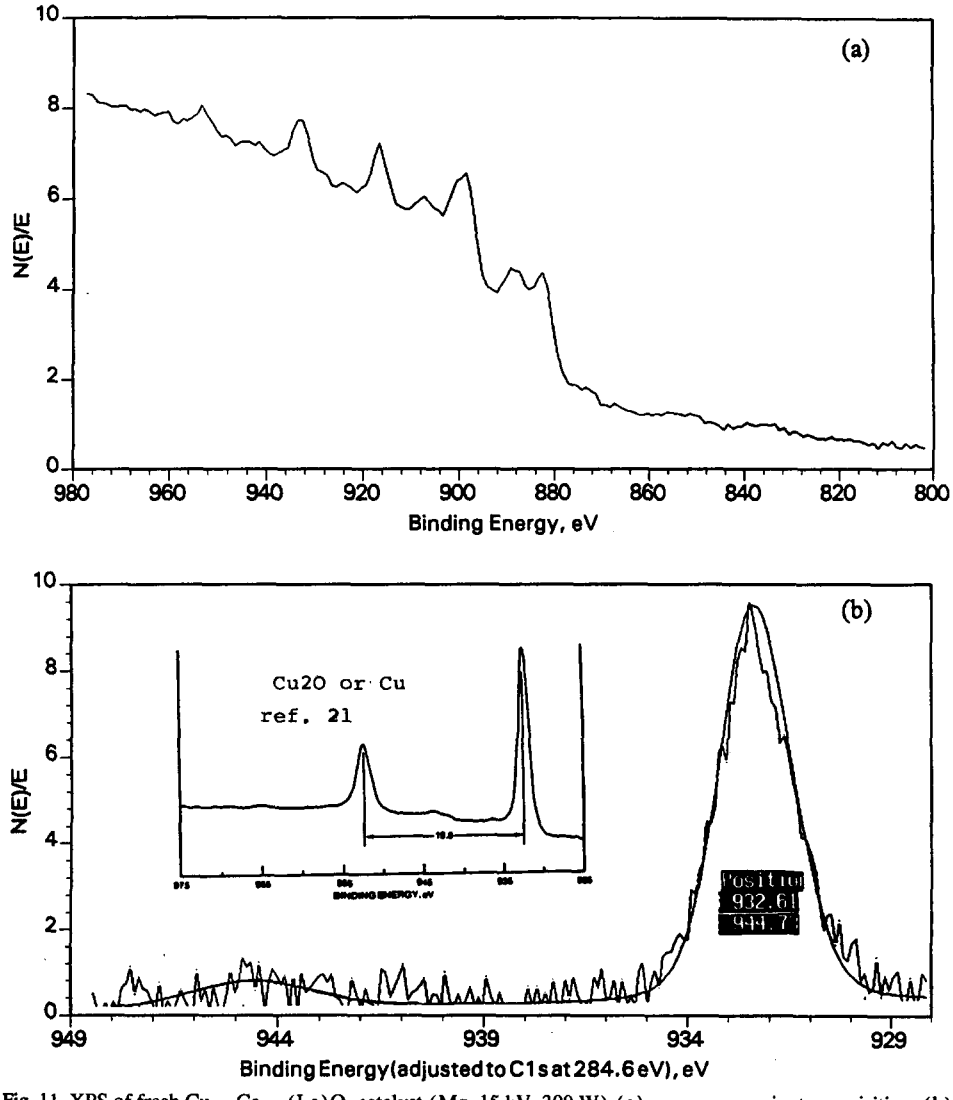

Fig. 11. XPS of fresh $Cu_{0.15}Ce_{0.85}(La)O_x$ catalyst (Mg, 15 kV, 300 W) (a) survey, one-minute acquisition; (b) forty-minute acquisition.

when a gas with 2% CO in He was used to scavenge a spent catalyst after the system had been flushed with helium. The COS level decreased exponentially with time.

3.6. *Characterization of the Cu–Ce–O catalysts*

X-ray powder diffraction analyses of the fresh composite Cu–Ce–O catalysts identified two crystal phases, fluorite-type and copper oxide, in catalysts containing over 20 at.-% copper, and only the fluorite structure in the composites containing less than 20 at.-% Cu. Also in the Y-doped and Cu-doped zirconia catalysts, only the fluorite-type structure was found. Two small copper oxide peaks were found in

Table 6
Binding energies of elements in the $Cu_{0.15}Ce_{0.85}(La)O_x$ catalyst determined by XPS (Mg, 15 kV, 300 W)

Element	Fresh (eV)	Used (eV)	Assignment[b]
Cu $2p_{3/2}$	932.7	932.4	Cu, Cu_2O, copper sulfide
Ce $3d_{5/2}$	881.9	882.4	CeO_2
O 1s	529.0	529.3 (72%)[a]	Metal oxide (CeO_2)
		531.7 (28%)	Metal sulfate, carbonate
S 2p	–	162.6 (74%)	Copper sulfide
		168.0 (26%)	Metal sulfate

[a]Peak area percent.
[b]Assignment based on the data in ref. [21].

the fresh 7.8 wt.-% CuO_x/CeO_2catalyst as shown in Fig. 9, but, these two peaks disappeared in the used catalyst. The distinct fluorite-type diffraction pattern was found in both the used and fresh Cu–Ce–O catalysts, which indicates that the fluorite oxide was stable in the present reaction conditions.

STEM analysis of the Cu-impregnated ceria identified many large copper oxide particles (ca. 100 nm) in the fresh catalyst, but relatively smaller particles on the used one as seen in Fig. 10. In Fig. 10, the left-hand-side top and bottom pictures are the dark field image of the fresh catalyst matrix and the bright field image of the used one, respectively, while the right-hand-side pictures are the corresponding elemental mapping images. Sulfur found on the used catalyst was always associated with copper. STEM analyses of the fresh Cu–Ce–O composite catalyst found the copper (oxide) as small particles (a few nm) and large agglomerates (> 10 nm), the latter increasing in population with the copper content. A higher number of small copper particles was found uniformly dispersed on the used composite catalyst and they were also extensively associated with sulfur.

Fig. 11 shows the XP spectra of the fresh $Cu_{0.15}Ce_{0.85}(La)O_x$ catalyst. Comparison with standard spectra [21] finds the Cu 2p satellite for the fresh catalyst similar to cuprous oxide(Cu_2O) or metallic copper and Ce 3d satellites for both fresh and used catalysts similar to bulk ceria. The Cu 2p spectra of the $CuO/\gamma\text{-}Al_2O_3$ are identical to CuO. But, the Cu 2p XPS of the CuO_x/CeO_2 is between the CuO and reduced CuO (Cu_2O or Cu). The binding energies of the $Cu_{0.15}Ce_{0.85}(La)O_x$ catalyst are summarized in Table 6. The double S 2p XPS peaks of the used catalyst

Table 7
Surface compositional analysis of $Cu_{0.15}Ce_{0.85}(La)O_x$ catalyst by XPS

Atomic ratio	Cu/Ce	S/Cu
Bulk material[a]	0.176	0
Fresh catalyst	0.133	0
Used catalyst	0.364	1.59
1 min Ar^+ sputtering	0.206	1.36
7 min Ar^+ sputtering	0.151	1.15

[a]Based on stoichiometry.

indicate two kinds of sulfur: metal sulfate and sulfide contributing to the high and low binding energies, respectively. The sulfide peak is a major peak. Similarly, two O 1s peaks were found in the XPS of the used catalyst. The peak of higher binding energy can be assigned to sulfate or carbonate, while the peak of low binding energy is assigned to metal oxide. The qualitative surface compositional analysis of the $Cu_{0.15}Ce_{0.85}(La)O_x$ catalyst by XPS is given in Table 7. The surface was enriched in copper after use. The Cu/Ce and S/Cu ratios decreased by argon ion sputtering of the surface, but the S/Cu did not reach a zero value because of interference from the catalyst pores.

4. Discussion

Previous studies have suggested that the reduction of sulfur dioxide by carbon monoxide proceeds via a redox mechanism [12,15,18].

$$\text{Cat}-[\ ]+SO_2 \rightarrow \text{Cat}-O+SO \quad (8)$$

$$\text{Cat}-O+CO \rightarrow \text{Cat}-[\ ]+CO_2 \quad (9)$$

$$\text{Cat}-[\ ]+SO \rightarrow \text{Cat}-O+S \quad (10)$$

Accordingly, the reaction is initiated by the creation of an oxygen vacancy. As an oxygen vacancy is created, SO_2 donates one oxygen to that vacancy to form a SO group. The SO may be mobile on the surface until it finds another vacancy to donate its oxygen or a vacancy may migrate to a neighboring site to accept its oxygen. High oxygen mobility in the catalyst would facilitate the oxygen transfer on the surface or from the bulk to the surface. Therefore, oxygen vacancy and mobility seem to be important properties for an active catalyst. The active catalysts previously reported [13–16], La–Ti–O and La–Co–O perovskite mixed oxides, generally possess such properties. Ceria and zirconia studied in this work are well known for their oxygen vacancy and mobility properties [19]. Ceria has a very stable fluorite-type structure, while the fluorite structure of zirconia can be stabilized by the use of oxide dopants. The oxygen vacancy in a fluorite oxide is created by replacing the metal ion (Ce^{4+}, Zr^{4+}) in the lattice with other di- or tri-valent metal ions. Rare earth zirconates ($Ln_2Zr_2O_7$) having oxygen mobility properties [20] were also found to be active catalysts in this work. All these results support the present mechanistic argument.

However, the oxygen vacancy can be taken up by other oxygen-containing molecules, such as CO_2 or H_2O. The stronger the association of these impurity oxidants with the vacancy, the more they will inhibit the reaction. Thus, creation of oxygen vacancies on the surface is a key step. Incorporation of alkaline and rare earth dopant oxides into the ceria lattice enhances the oxygen vacancy concentration and mobility [19]. But, the created vacancies are usually capped by an outside oxygen and the strong vacancy-dopant ion association stabilizes the capping oxy-

gen. The capping oxygen has to be removed to bring about oxygen vacancy and initiate the redox reaction. For ceria, temperature-programmed reduction by hydrogen [22] has found that the surface capping oxygen can be removed at about 500°C. Higher reduction temperature may be needed in the presence of SO_2 due to its strong bonding to the surface. It is also known that CO adsorption on ceria is inhibited by water [23,24]. The introduction of transition metals may provide surface sites for CO adsorption and facilitate the reduction of the fluorite oxide surface through strong metal–support interaction as found in the Pt–CeO_2 [22] system:

$$\text{Cat}-\text{M}--\text{CO}+\text{Cat}-\text{O}\rightarrow\text{Cat}-\text{M}+\text{Cat}-[\ ]+\text{CO}_2 \qquad (11)$$

Cat-[ ] can further react according to the redox reaction scheme (8)–(10). This assumption was validated by the fact that the catalytic activity of ceria or zirconia and resistance to water or carbon dioxide poisoning were significantly enhanced by the addition of transition metals, such as copper. XPS studies showed that copper in the Cu–Ce–O catalyst tends to be stabilized in a reduced oxidation state (Cu_2O or Cu^0) instead of CuO, while it is well known that CO strongly adsorbs on Cu^{1+} ion. Preliminary temperature-programmed reduction experiments indicated that addition of copper can initiate the reduction of surface capping oxygen of ceria at low temperature. These data suggest that there is a strong interaction between copper (oxide) and ceria. For the Cu–Ce–O system, both coprecipitation and impregnation preparation methods gave rise to an active catalyst. The catalyst activity was not sensitive to the copper content, but the selectivity tended to decrease with the copper content. XRD analysis identified the CuO phase when the copper content was over 20 at%. STEM analysis revealed bimodal size distribution of copper on ceria. We postulate that only a certain amount of copper is needed to promote the catalytic properties of ceria, and the excess copper (oxide) can form aggregates. Presently, we do not have enough data to clarify the copper particle size effect. Further work to elucidate the interaction of copper with ceria is underway.

As reported in the literature [15,17], the transition metal will likely be sulfided by the elemental sulfur product:

$$\text{Cat}-\text{M}+\text{S}_x\rightarrow\text{Cat}-\text{MS}_x \qquad (12)$$

Copper sulfide was found on a used Cu–Ce–O catalyst by XPS surface compositional analysis, but was not detected by XRD analysis, possibly because it is dispersed in ceria in amorphous form or because copper sulfide crystals did not grow on the stable ceria surface. The fluorite oxide showed high stability in the present study. For example, ceria kept its fluorite-type crystal structure after a 48 h test run. STEM elemental mapping showed that the sulfur on the catalyst was extensively associated with copper. The formation of copper sulfide extracted copper from the bulk so that the surface was enriched in copper on the used catalyst. Copper sulfide may play a similar role to copper in promoting the reducibility of the fluorite oxide. But, the deposited sulfur may react with CO to form COS through following equation:

$$Cat-MS_x+CO \rightarrow Cat-M+COS \quad (13)$$

Therefore, an adsorbed CO molecule can pick up oxygen through Eq. (9) and sulfur through Eq. (13). We believe that COS formation is the result of these two competitive processes and it prevails in the following two cases: (i) when excess CO exists and the oxidant is not sufficient to oxidize it, the extra CO reacts with sulfur to form COS; (ii) when the surface oxygen is more strongly bound than sulfur, the adsorbed CO picks up sulfur to form COS. This reasoning is evidenced by the COS evolution profiles shown in Figs. 7 and 8. In Fig. 7, COS formation proceeded significantly at initial reaction times when the catalyst was not activated or the surface oxygen was not mobile, decreasing to zero at fully activated state, while a small amount of COS was formed at a later reaction time. The latter must be the result of reaction of a small amount of CO with the sulfur deposited on the catalyst surface. The reaction of CO and the deposited sulfur is further illustrated by Fig. 8, where COS evolution profiles are shown for 2% CO/He scavenging of the used catalysts following a helium flush. A simple exponential decay of $COS(t)$ predicted by assuming a formation rate $r_{COS}=k_s[S]_{surf}P_{CO}$ fits well the data of Fig. 8.

5. Conclusion

In this work, we have found that fluorite-type oxides, such as ceria and zirconia, are active catalysts for the reduction of sulfur dioxide by carbon monoxide with high selectivity to elemental sulfur over carbonyl sulfide. The activity of these oxides may result from their high oxygen vacancy concentration and mobility properties which are needed for a redox reaction mechanism. Addition of active transition metals such as copper to the fluorite oxide significantly lowered the reaction light-off temperature and enhanced the catalyst resistance toward water and carbon dioxide poisoning. Analyses of the Cu–Ce–O system showed that the fluorite crystal structure of ceria is stable at the present reaction conditions and copper is stabilized in the ceria matrix. An active Cu–Ce–O catalyst can be prepared by either coprecipitation or impregnation. The catalyst activity is not sensitive to the copper content. The Cu–Ce–O composite surface was enriched in copper and a surface copper sulfide was found in the used catalyst. Further characterization and systematic composition studies of this catalyst system are underway to clarify the type of metal-fluorite oxide interaction that leads to the enhanced activity reported here.

Acknowledgements

We thank Dr. A.J. Garratt-Reed for the STEM and Mr. J. Martin for the XPS analyses. This work has been financially supported by the US Department of Energy under the University Coal Research Program, Grant No. DE-FG22-92PC92534.

References

[1] J.B. Pfeiffer, Sulfur Removal and Recovery Industrial Processes, Adv. Chem. Ser., No. 139, Am. Chem. Soc., Washington, DC, 1975.
[2] K.V. Kwong, R.E. Merssner and C.C. Hong, in Proc. of the SO_2 Control Symposium, Washington, DC, December 3–6, 1991, Vol. 2, Session 5B, Paper 8.
[3] P.R. Ryason and J. Harkins, J. Air Pollut. Control Assoc., 17 (1967) 796–799.
[4] S.E. Khalafalla, E.F. Foerster and L.A. Haas, Ind. Eng. Chem., Prod. Res. Dev., 10 (1971) 133–137.
[5] S.E. Khalafalla and L.A. Haas, in J.B. Pfeiffer (Editor), Sulfur Removal and Recovery Industrial Processes, Adv. Chem. Ser., No. 139, Am. Chem. Soc., Washington, DC, 1975, pp. 60–64.
[6] L.A. Haas and S.E. Khalafalla, J. Catal., 29 (1973) 264–269.
[7] L.A. Haas and S.E. Khalafalla, J. Catal., 30 (1973) 451–459.
[8] R. Querido and W.L. Short, Ind. Eng. Chem., Process Des. Dev., 12 (1973) 10–18.
[9] V.C. Okay and W.L. Short, Ind. Eng. Chem., Process Des. Dev., 12 (1973) 291–294.
[10] L. Bajars, US Patent 3 978 200 (1976).
[11] J. Happel, M.A. Hnatow, L. Bajars and M. Kundrath, Ind. Eng. Chem., Prod. Res. Dev., 14 (1975) 154–158.
[12] J. Happel, A.L. Leon, M.A. Hnatow and L. Bajars, Ind. Eng. Chem., Prod. Res. Dev., 16 (1977) 150–154.
[13] J.M. Whelan, US Patent 4 081 519 (1977).
[14] D.B. Hibbert and R.H. Campbell, Appl. Catal., 41 (1988) 273–287.
[15] D.B. Hibbert and R.H. Campbell, Appl. Catal., 41 (1988) 289–299.
[16] D.B. Hibbert, Catal. Rev. Sci. Eng., 34 (1992) 391–408.
[17] J.A. Baglio, Ind. Eng. Chem. Prod. Res. Dev., 21 (1982) 38–41.
[18] W. Liu and M. Flytzani-Stephanopoulos, in J.N. Armor (Editor), Environmental Catalysis, Am. Chem. Soc., Symp. Ser., Vol. 552, Am. Chem. Soc., Washington, DC, 1994, pp. 375–392.
[19] P. Hagemuller and W. Van Gool, Solid Electrolytes, Academic Press, New York, 1978.
[20] H.L. Tuller and P.K. Moon, Mater. Sci. Engrg. B1, (1988) 171–191.
[21] C.D. Wagner, W.M. Rigg, L.E. Davis, J.F. Moulder and G.E. Muilenberg, Handbook of X-ray Photoelectron Spectroscopy, Perkin-Elmer, Eden Prairie, MN, 1978.
[22] H.C. Yao and Y.F.Y. Yao, J. Catal., 86 (1984) 254–265.
[23] C. Li, Y. Sakata, T. Arai, K. Domen, K. Maruya and T. Onishi, J. Chem. Soc., Faraday Trans. 1, 85 (1989) 929–943.
[24] C. Li, Y. Sakata, T. Arai, K. Domen, K. Maruya and T. Onishi, J. Chem. Soc., Faraday Trans. 1, 85 (1989) 1451–1461.